Atomic-orbital analysis of the Ni(111) Fermi surface by two-dimensional photoelectron spectroscopy with linearly polarized synchrotron radiation

Yukari Fujioka[1], Masaru Takizawa[2], Hidetoshi Namba[1], Fumihiko Matsui[3], and Hiroshi Daimon[3]

1) Department of Physical Sciences, Faculty of Science and Engineering, Ritsumeikan University, Kusatsu, Shiga 525-8577, Japan.

2) Research Organization of Science and Engineering, Ritsumeikan University, Kusatsu, Shiga 525-8577, Japan.

3) Graduate School of Materials Science, Nara Institute of Science and Technology, Ikoma, Nara 630-0192, Japan.

Abstract

We have performed two-dimensional photoelectron spectroscopy measurement on Ni(111) surface. A two-dimensional photoelectron intensity angular distribution (2D-PIAD) from the Ni(111) surface was obtained using a display-type analyzer and the linearly polarized synchrotron radiation. 2D-PIAD showed the symmetry-lowered pattern due to the polarization vector of SR light. This suggests that the Fermi surface of Ni(111) is constituted by a mixture of d_{xy}, d_{yz}, d_{zx} atomic orbital components; T_{2g} orbital.

1. Introduction

The transition metal Ni has attracted much attention because of its interesting electronic, magnetic, and chemisorption properties. The electronic structures have been extensively studied so far. For example, photoelectron spectroscopy (PES) measurements have shown the narrower Ni 3*d* band width than that of the theoretical calculation and the satellite structure located around 6 eV below the Ni 3*d* bands, which have been explained by the strong electron correlation effect [1]. Furthermore, angle-resolved photoelectron spectroscopy (ARPES) measurements have directly revealed the band structure and its renormalization due to the strong electron correlation effect [2, 3]. Moreover, temperature dependent ARPES measurements have revealed that the exchange splitting vanishes above T_C [4], i.e., a Stoner-like behavior of the exchange splitting. In addition, a surface state has been also identified on the Ni(111) surface [5] and they have been revealed to be exchange split by spin-resolved ARPES measurements [6]. Furthermore, on the stepped surface of Ni(755) [= 6(111) × (100)], one-dimensional surface state was found at the step edge [7] maybe due to the interaction with the *d* orbital character [8]. However, the information on the atomic orbital has not been so much studied. Recently, an atomic orbital analysis of the Cu Fermi surface (FS) has been performed and revealed that the FS is composed of mainly 4*p* orbitals with their axes pointing outward [9]. In the present study, we have performed the atomic-orbital analysis of Ni(111) by two-dimensional photoelectron spectroscopy (2D-PES) measurement utilizing the linearly polarized synchrotron radiation (SR) light.

2. Experiment

The experiment was performed at the linearly polarized soft x-ray beamline BL-7 of SR center, Ritsumeikan University [10]. The electric vector of the linearly polarized SR light was in the horizontal plane and incident on the sample normal. The Ni(111) single crystal sample was cleaned *in situ* by repeated cycles of Ar^+ bombardment and annealing to ~ 800 °C in an ultrahigh-vacuum chamber to obtain a clean surface. The surface quality was checked by low energy electron diffraction and Auger electron spectroscopy measurements. The 2D-PES measurements were performed at room temperature under ultrahigh vacuum of ~ 1×10^{-8} Pa using a two-dimensional display-type spherical mirror analyzer (DIANA) [11, 12] with SR light. A two-dimensional photoelectron intensity angular distribution (PIAD) and a stereo profile of the FS are efficiently obtained by using DIANA. 2D-PIAD of this

experiment was collected by energy window of 100 meV. Typical acquisition time for one PIAD was 30 sec. The total energy resolution was about 400 meV. The angular resolution was about 1◦.

3. Results

Figure 1 (a) shows the angle-integrated spectrum of Ni(111) taken with $h\nu$ = 45 eV. The bands near the Fermi level are mainly composed of Ni 3*d* states and the structure around -6 eV is a two-hole-bound state [1]. The contamination peak around -10 eV was very weak, also confirming the sample surface cleanness. As shown in Fig. 1, the series of PIAD change with energy, reflecting the band dispersion of Ni 3*d*. However, the symmetry of the PIAD pattern was different from the expected one with a three-fold symmetry due to the face-centered-cubic (fcc) crystal structure of Ni. This is due to the matrix element effect of the incident linearly polarized SR light. This effect is discussed below. By rotating the sample around the (111) surface normal, the angle-dependent PIADs near the Fermi level were obtained. As shown in Fig. 2, the PIADs rotates clockwise with increasing the azimuth angle ϕ. By applying mirror

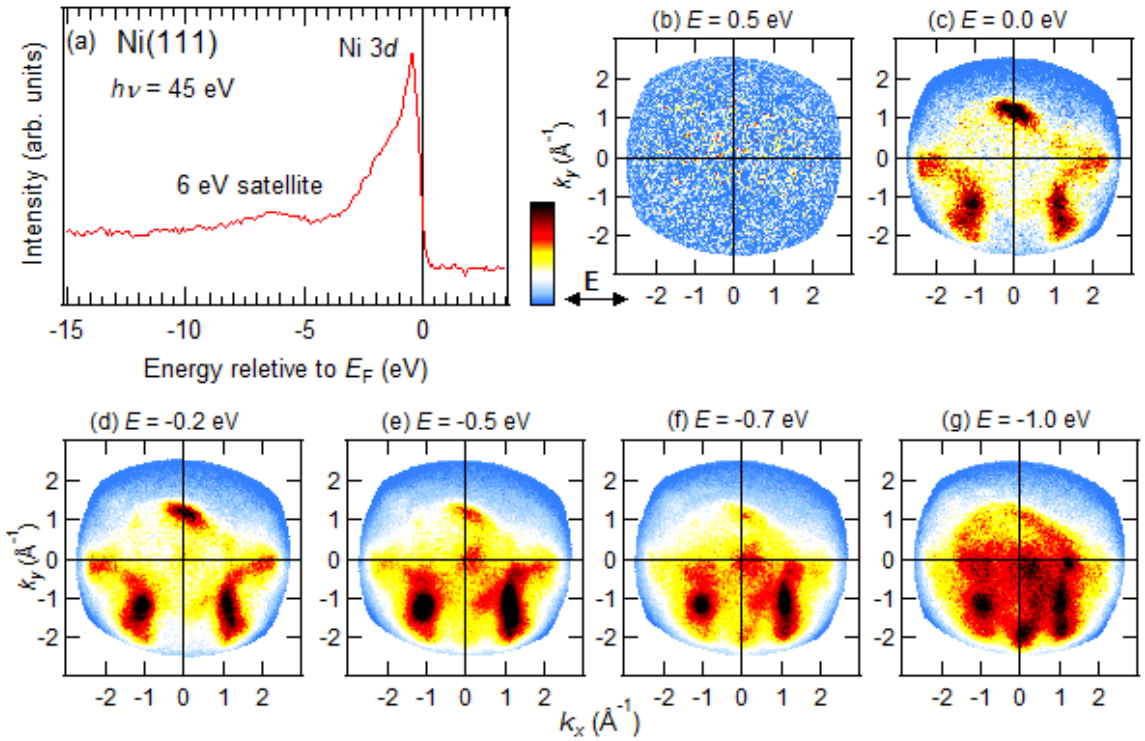

Fig. 1 2D-PES result of Ni(111) taken with $h\nu$ = 45 eV. (a) Angle-integrated PES spectrum. The PIADs at E = 0.5 eV (b), 0.0 eV (c), -0.2 eV (d), -0.5 eV (e), -0.7 eV (f), and -1.0 eV (g). The electric vector of the incident light is in the horizontal direction.

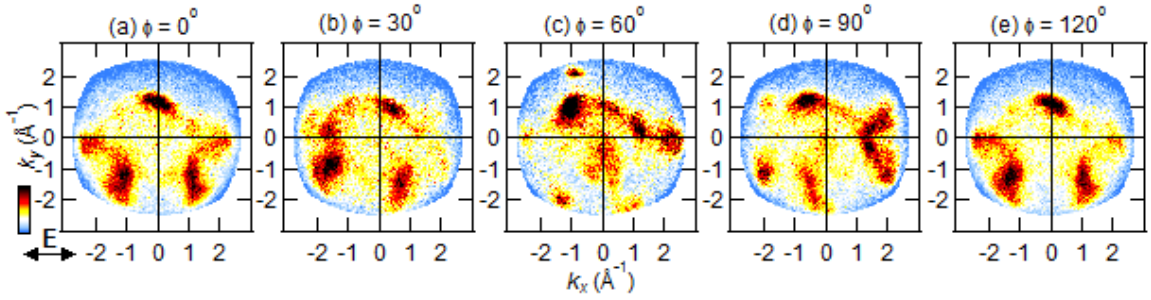

Fig. 2 Angle-dependent PIADs at the Fermi level (E = 0.0 eV) taken with $h\nu$ = 45 eV. The PIADs of ϕ = 0° (a), 30° (b), 60° (c), 90° (d), and 120° (e).

symmetry operation horizontally to the photoelectron pattern shown in Fig. 2(b), we obtained a pattern which is very similar to that of Fig. 2(d). Similarly, by applying mirror symmetry operation vertically to the photoelectron pattern shown in Fig. 2(a), we obtained a pattern resembling that of Fig. 2(c). Finally, the PIAD of ϕ = 120° [Fig. 2(e)] coincides with that of ϕ = 0° [Fig. 2(a)]. This indicates that the measured electronic structure indeed has a three-fold symmetry due to the fcc crystal structure of

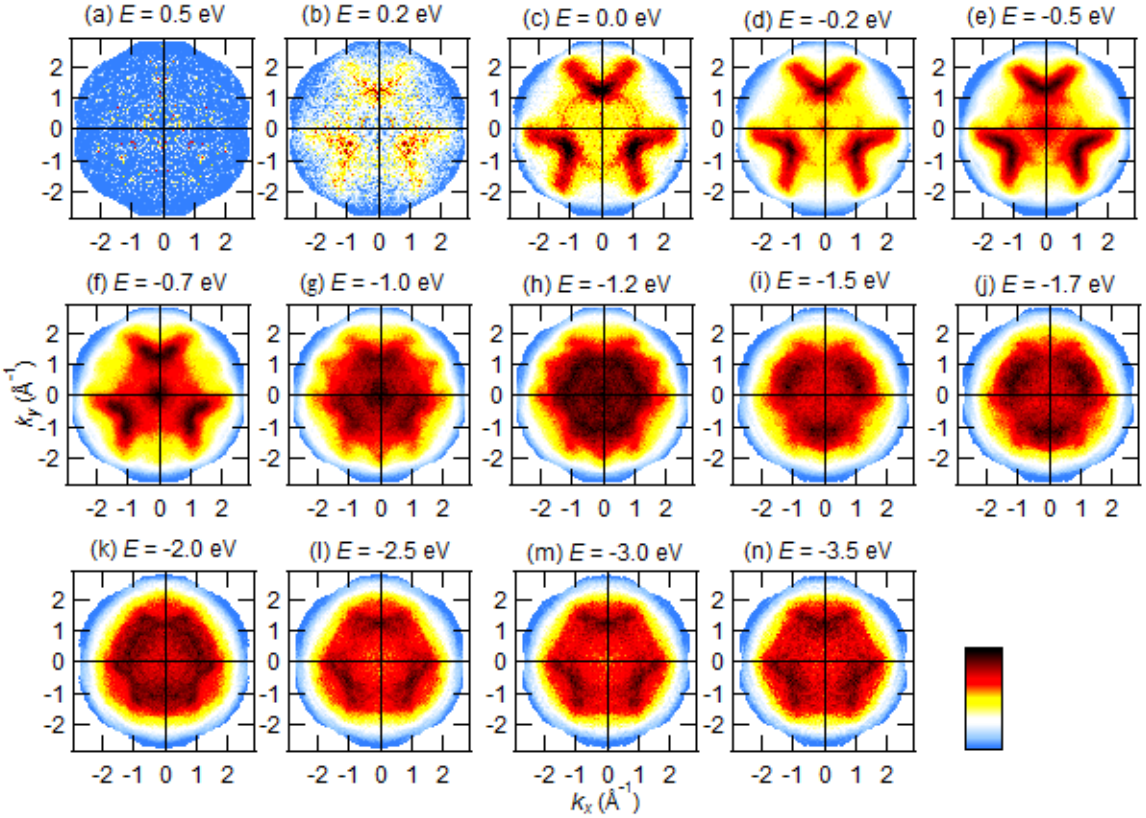

Fig. 3 Constant energy surfaces of Ni(111) at various energies by applying the three-fold symmetry to the PIADs taken with $h\nu$ = 45 eV. E = 0.5 eV (a), 0.2 eV (b), 0.0 eV (c), -0.2 eV (d), -0.5 eV (e), -0.7 eV (f), -1.0 eV (g), -1.2 eV (h), -1.5 eV (i), -1.7 eV (j), -2.0 eV (k), -2.5 eV (l), -3.0 eV (m), and -3.5 eV (n).

Ni. From these results, we concluded that the Ni bulk band structure was successfully obtained. By applying the three-fold symmetry to the observed PIADs, the band structure of Ni(111) was obtained as shown in Fig. 3. With decreasing the energy, the electronic structures move to the center [Fig. 3(c-h)], then move back to outer region [Fig. 3(h-n)]. This behavior seems to be consistent with the calculated band structure of Ni [13] (shown in Fig. A1), where the bands gather to Γ point and then move to X or K points with decreasing the energy from the Fermi level.

4. Discussion

The analysis of two-dimensional PIAD from a tight-binding approximated valence band and a Bloch-wave final state showed that the photoelectron intensity $I(\theta_k, \phi_k)$ in the direction of polar angle θ_k and azimuth angle ϕ_k can be expressed as [9, 14]:

$$I(\theta_k, \phi_k) \sim D^1(k_{//}) \, |\Sigma_\nu A_\nu|^2,$$

where $D^1(k_{//})$ is the one-dimensional density of states [15] and A_ν is the "angular distribution from the ν-th atomic orbital" [16].

First, the $D^1(k_{//})$ was obtained using the semiempirical band structure calculation [13]. The basis set contains five tight-binding *d*-wave functions and four orthogonalized plane waves (OPWs). The calculated FSs (energy window of 100 meV) and the corresponding *k*-trace are shown in Fig. 4. Here, the work function of the sample ϕ = 5.2 eV [5] and the inner potential V_0 = 10.7 eV [17] have been used to obtained the momentum perpendicular to the surface, assuming free electron final states. The calculated FS taken with $h\nu$ = 21.2 eV [Fig. 4(a)] is similar to that of the layer Korringa-Kohn-Rostoker calculation [4], confirming the validity of the calculation to

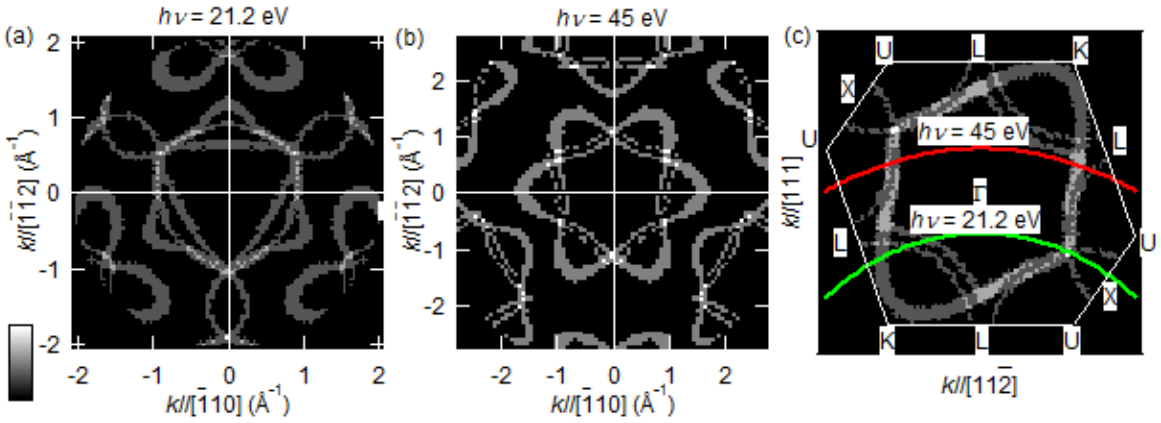

Fig. 4 Calculated Fermi surfaces for Ni. (a) The Ni(111) Fermi surface taken with $h\nu$ = 21.2 eV. (b) The Ni(111) Fermi surface taken with $h\nu$ = 45 eV. (c) Traces in *k* space with the Fermi surface.

some extent. Therefore, we can compare the experimental FS with this calculated FS. Compared with the experimentally obtained and symmetrized FS [Fig. 3(c)], the calculated FS taken with $h\nu$ = 45 eV [Fig. 4(b)] shows more complicated structures. This may be due to the lack of polarization vector normal to the surface.

Next, the $|A_v|^2$ from each d orbital was calculated according to Ref. [16]. As in the experimental condition, the linearly polarized SR light is incident from [111] direction. As shown in Fig. 5, the angular distribution from an atomic orbital is not uniform but unique to the atomic orbital due to the relation between the polarization vector of the incident SR and the atomic orbital. Therefore, comparing the experimental PIAD with these angular distributions from the atomic orbitals, one can determined the atomic orbitals constituting the FS.

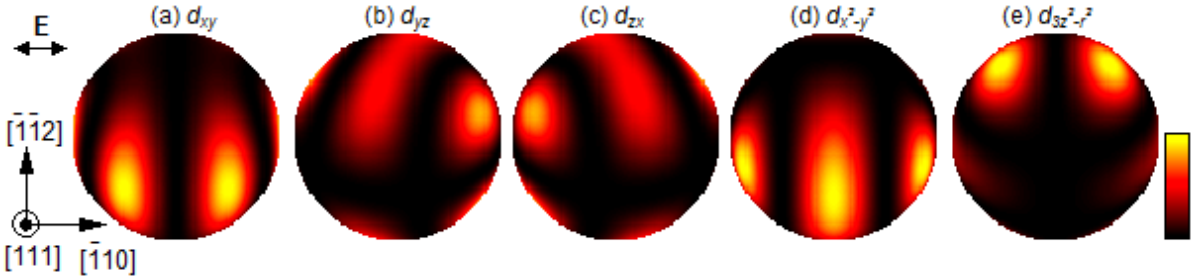

Fig. 5 Calculated angular distribution from each d atomic orbital [16]. (a) d_{xy}. (b) d_{yz}. (c) d_{zx}. (d) $d_{x^2-y^2}$. (e) $d_{3z^2-r^2}$.

By multiplying the $D^1(k_{//})$ [Fig. 4] and the $|A_v|^2$ [Fig. 5], simulated PIADs for the Ni(111) FS taken with $h\nu$ = 45 eV are obtained [Fig. 6]. The simulated PIAD for d_{xy} orbital [Fig. 6(a)] shows strong structures around bottom left and bottom right, that for d_{yz} orbital [Fig. 6(b)] shows strong structures around middle right and top center, that for d_{zx} orbital [Fig. 6(c)] shows strong structures around middle left and top center, that for $d_{x^2-y^2}$ orbital [Fig. 6(d)] shows strong structures around middle left, bottom center, and middle right, and that for $d_{3z^2-r^2}$ orbital [Fig. 6(e)] shows strong structures around top left and top right. As shown in Fig. 1(c), the experimental FS shows strong

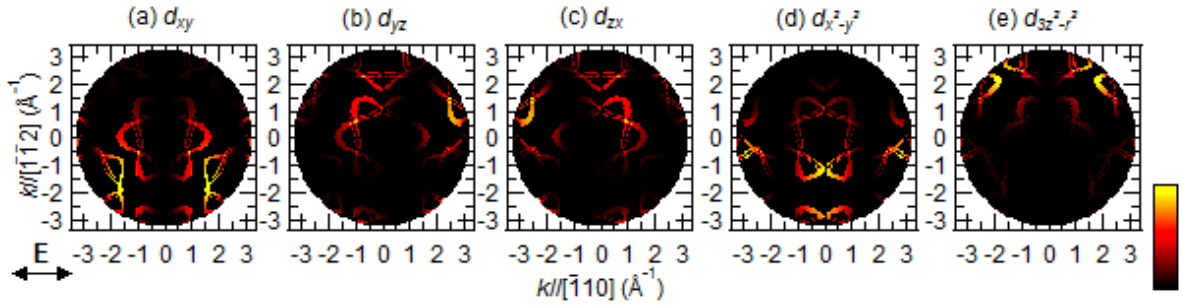

Fig. 6 Simulated PIADs for the Ni(111) FS taken with $h\nu$ = 45 eV. The FS is assumed to be composed of each d atomic orbital; (a) d_{xy}, (b) d_{yz}, (c) d_{zx}, (d) $d_{x^2-y^2}$, and (e) $d_{3z^2-r^2}$.

structures around bottom and middle left, bottom and middle right, and top center. Therefore, the experimentally observed strong structures around bottom and middle left is considered to come from d_{xy} and d_{zx} orbitals, those around bottom and middle right come from d_{xy} and d_{yz} orbitals, and that around top center come from d_{yz} and d_{zx} orbitals.

The atomic orbital components constituting the Ni(111) FS are also evaluated by considering the eigenvectors in the above mentioned semiempirical band structure calculation. Figure 7 shows the calculated contribution from each atomic orbital for the Ni(111) FS taken with $h\nu$ = 45 eV. The bottom part of FS is mainly composed of d_{xy} orbital, the top right part is composed of d_{yz} orbital, and the top left part is composed of d_{zx} orbital. The calculated atomic orbital distribution shows good agreement with the result of the atomic-orbital analysis from present measured PIADs.

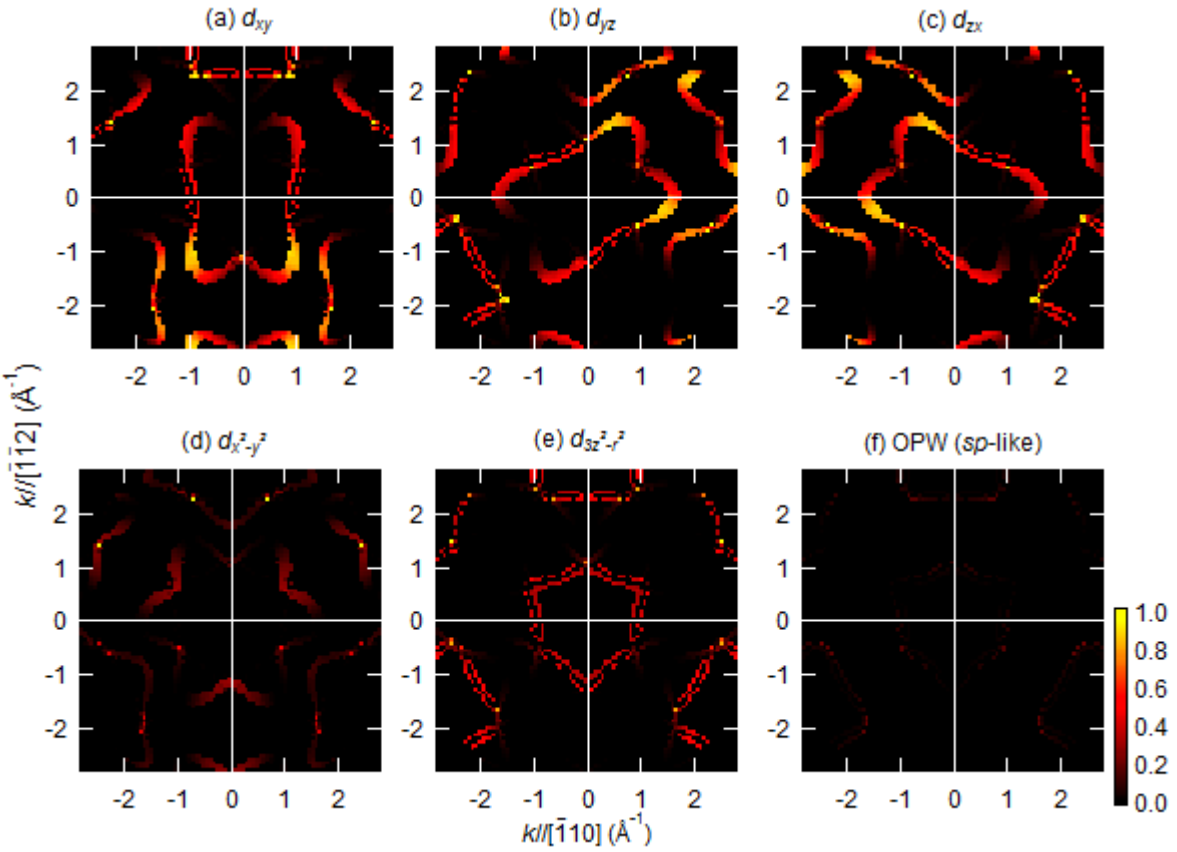

Fig. 7 Calculated contribution from each atomic orbital to the Ni(111) FS taken with $h\nu$ = 45 eV. (a) d_{xy}. (b) d_{yz}. (c) d_{zx}. (d) $d_{x^2-y^2}$. (e) $d_{3z^2-r^2}$. (f) Four OPWs, that is, *sp*-like component.

5. Conclusions

We have performed two-dimensional photoelectron spectroscopy measurements on

Ni(111) surface. We have observed the Ni(111) Fermi surface which has a three-fold symmetry due to the face-centered-cubic crystal structure of Ni. The photoelectron intensity angular distribution (PIAD), however, showed symmetry-lowered pattern due to the relation between the polarization vector of the incident synchrotron radiation and the atomic orbitals constituting the Ni(111) Fermi surface. Compared with the simulated PIADs from the atomic orbitals, it is suggested that the Ni(111) Fermi surface is constituted by a mixture of d_{xy}, d_{yz}, d_{zx} orbital components; T_{2g} orbital.

Acknowledgment

This work was partly supported by Open Research Center Project for Private Universities matching fund subsidy from MEXT, 2007-2011.

Appendix: Semiempirical band structure calculation for Ni

The basis set is 4 orthogonal plane waves (OPWs) and 5 tight-binding d wave functions [13]:

$$\phi_1 = |\mathbf{k} + \mathbf{K}_1>,\ \phi_2 = |\mathbf{k} + \mathbf{K}_2>,\ \phi_3 = |\mathbf{k} + \mathbf{K}_3>,\ \phi_4 = |\mathbf{k} + \mathbf{K}_4>,$$
$$\phi_5 = |d_{xy}>,\ \phi_6 = |d_{yz}>,\ \phi_7 = |d_{zx}>,\ \phi_8 = |d_{x^2-y^2}>,\ \phi_9 = |d_{3z^2-r^2}>,$$

where $\mathbf{K}_1 = (0,0,0)$, $\mathbf{K}_2 = 2\pi/a(0,-2,0)$, $\mathbf{K}_3 = 2\pi/a(-1,-1,-1)$, $\mathbf{K}_4 = 2\pi/a(-1,-1,0)$, and a is the lattice constant (a = 3.52 Å for Ni). Note that the calculation is performed in the 1/48th Brillouin zone ($2\pi/a \geq k_y \geq k_x \geq k_z \geq 0$). The 9×9 Hamiltonian is expressed as

$$H = \begin{pmatrix} H_{cc} & H_{cd} \\ H_{cd}^{\dagger} & H_{dd} \end{pmatrix},$$

where H_{cc} is a 4×4 OPW block, H_{dd} is a 5×5 tight-binding d block, and H_{cd} is a 4×5 hybridization block. The OPW block is expressed as

$$H_{cc} = \begin{pmatrix} \beta+\alpha|\mathbf{k}(8a/2\pi)|^2 & V_{200}F_{0\text{-}20} & V_{111}F_{\text{-}1\text{-}1\text{-}1} & V_{111}F_{\text{-}1\text{-}11} \\ V_{200}F_{0\text{-}20} & \beta+\alpha|(\mathbf{k}+\mathbf{K}_2)(8a/2\pi)|^2 & V_{111}F_{0\text{-}20}F_{\text{-}1\text{-}1\text{-}1} & V_{111}F_{0\text{-}20}F_{\text{-}1\text{-}11} \\ V_{111}F_{\text{-}1\text{-}1\text{-}1} & V_{111}F_{0\text{-}20}F_{\text{-}1\text{-}1\text{-}1} & \beta+\alpha|(\mathbf{k}+\mathbf{K}_3)(8a/2\pi)|^2 & V_{200}F_{\text{-}1\text{-}1\text{-}1}F_{\text{-}1\text{-}11} \\ V_{111}F_{\text{-}1\text{-}11} & V_{111}F_{0\text{-}20}F_{\text{-}1\text{-}11} & V_{200}F_{\text{-}1\text{-}1\text{-}1}F_{\text{-}1\text{-}11} & \beta+\alpha|(\mathbf{k}+\mathbf{K}_4)(8a/2\pi)|^2 \end{pmatrix},$$

where β and α are the bottom and the curvature of the free-electron bands, respectively, V_{111} and V_{200} are pseudopotential coefficients, and F_{000}, $F_{0\text{-}20}$, $F_{\text{-}1\text{-}1\text{-}1}$, $F_{\text{-}1\text{-}10}$ are the symmetrizing factors. These symmetrizing factors are assumed as follows [18]:

$$F_{000} = 1,$$
$$F_{0\text{-}20} = [\sin(\pi/2\ (k_y - k_x)/(4\pi/a - k_x - k_y))]^{1/2},$$
$$F_{\text{-}1\text{-}1\text{-}1} = [\sin(\pi/2\ (k_x + k_z)/(3\pi/a - k_y))]^{1/2},$$

$$F_{-1-10} = [\sin(\pi/2\ (k_x - k_z)/(3\pi/a - k_y))]^{1/2}.$$

The tight-binding *d* block is expressed as [19]

H_{dd} =

$$\begin{pmatrix}
E_0 \pm \sigma_{t2g} \\ -4A_1\cos\xi\cos\eta \\ +4A_2\cos\zeta \\ \times(\cos\xi+\cos\eta) & -4A_3\sin\xi\sin\zeta & -4A_3\sin\eta\sin\zeta & 0 & -8/\sqrt{3}\ A_6\sin\xi\sin\eta \\
-4A_3\sin\xi\sin\zeta & E_0 \pm \sigma_{t2g} \\ -4A_1\cos\eta\cos\zeta \\ +4A_2\cos\xi \\ \times(\cos\eta+\cos\zeta) & -4A_3\sin\xi\sin\eta & -4A_6\sin\eta\sin\zeta & 4/\sqrt{3}\ A_6\sin\eta\sin\zeta \\
-4A_3\sin\eta\sin\zeta & -4A_3\sin\xi\sin\eta & E_0 \pm \sigma_{t2g} \\ -4A_1\cos\xi\cos\zeta \\ +4A_2\cos\eta \\ \times(\cos\xi+\cos\zeta) & 4A_6\sin\xi\sin\zeta & 4/\sqrt{3}\ A_6\sin\xi\sin\zeta \\
0 & -4A_6\sin\eta\sin\zeta & 4A_6\sin\xi\sin\zeta & E_0+\Delta \pm \sigma_{eg} \\ +4A_4\cos\xi\cos\eta \\ -4A_5\cos\zeta \\ \times(\cos\xi+\cos\eta) & 4/\sqrt{3}\ (A_4+A_5)\cos\zeta \\ \times(\cos\eta-\cos\xi) \\
-8/\sqrt{3}\ A_6\sin\xi\sin\eta & 4/\sqrt{3}\ A_6\sin\eta\sin\zeta & 4/\sqrt{3}\ A_6\sin\xi\sin\zeta & 4/\sqrt{3}\ (A_4+A_5)\cos\zeta \\ \times(\cos\eta-\cos\xi) & E_0+\Delta \pm \sigma_{eg} \\ -4/3\ (A_4+4A_5) \\ \times\cos\xi\cos\eta \\ +4/3\ (2A_4-A_5) \\ \times\cos\zeta(\cos\xi+\cos\eta)
\end{pmatrix},$$

where $\xi = k_x a/2$, $\eta = k_y a/2$, $\zeta = k_z a/2$, E_0 is the energy of t_{2g}, Δ is the crystal field, $2\sigma_{t2g}$ and $2\sigma_{eg}$ are the exchange splitting for t_{2g} and e_g, respectively, and A_i (i = 1,…,6) are the Fletcher parameters. It would be worthy to mention that these Fletcher parameters are related to the Slater-Koster parameters as follows [20]:

$$A_1 = -E_{xy\ xy}(110) = -3/4\ (dd\sigma) - 1/4\ (dd\delta),$$
$$A_2 = E_{xy\ xy}(011) = 1/2\ (dd\pi) + 1/2\ (dd\delta),$$
$$A_3 = E_{xy\ xz}(011) = 1/2\ (dd\pi) - 1/2\ (dd\delta),$$
$$A_4 = E_{x^2-y^2\ x^2-y^2}(110) = (dd\pi),$$
$$A_5 = -1/4\ E_{x^2-y^2\ x^2-y^2}(110) - 3/4\ E_{3z^2-r^2\ 3z^2-r^2}(110) = -3/16\ (dd\sigma) - 1/4\ (dd\pi) - 9/16\ (dd\delta),$$
$$A_6 = \sqrt{3}/2\ E_{xy\ 3z^2-r^2}(110) = -3/8\ (dd\sigma) - 3/8\ (dd\delta).$$

The hybridization block is expressed as [20]

H_{cd} =

$B_2 j_2(B_1\|\mathbf{k}\|b)$ $\times k_x k_y/\|\mathbf{k}\|^2$	$B_2 j_2(B_1\|\mathbf{k}\|b)$ $\times k_y k_z/\|\mathbf{k}\|^2$	$B_2 j_2(B_1\|\mathbf{k}\|b)$ $\times k_z k_x/\|\mathbf{k}\|^2$	$B_2 j_2(B_1\|\mathbf{k}\|b)$ $\times(k_x^2-k_y^2)/(2\|\mathbf{k}\|^2)$	$B_2 j_2(B_1\|\mathbf{k}\|b)$ $\sqrt{3}/6(3k_z^2/\|\mathbf{k}\|^2$ $- 1)$
$B_2 j_2(B_1\|(\mathbf{k}+\mathbf{K}_2)\|b)$ $\times[(\mathbf{k}+\mathbf{K}_2)_x$ $\times(\mathbf{k}+\mathbf{K}_2)_y$ $/\|\mathbf{k}+\mathbf{K}_2\|^2]\ F_{0\text{-}20}$	$B_2 j_2(B_1\|(\mathbf{k}+\mathbf{K}_2)\|b)$ $\times[(\mathbf{k}+\mathbf{K}_2)_y$ $\times(\mathbf{k}+\mathbf{K}_2)_z$ $/\|\mathbf{k}+\mathbf{K}_2\|^2]\ F_{0\text{-}20}$	$B_2 j_2(B_1\|(\mathbf{k}+\mathbf{K}_2)\|b)$ $\times[(\mathbf{k}+\mathbf{K}_2)_z$ $\times(\mathbf{k}+\mathbf{K}_2)_x$ $/\|\mathbf{k}+\mathbf{K}_2\|^2]\ F_{0\text{-}20}$	$B_2 j_2(B_1\|(\mathbf{k}+\mathbf{K}_2)\|b)$ $\times[((\mathbf{k}+\mathbf{K}_2)_x^2$ $-(\mathbf{k}+\mathbf{K}_2)_y^2)$ $/(2\|\mathbf{k}+\mathbf{K}_2\|^2)]\ F_{0\text{-}20}$	$B_2 j_2(B_1\|(\mathbf{k}+\mathbf{K}_2)\|b)$ $\sqrt{3}/6(3(\mathbf{k}+\mathbf{K}_2)_z^2$ $/\|\mathbf{k}+\mathbf{K}_2\|^2 - 1)\ F_{0\text{-}20}$
$B_2 j_2(B_1\|(\mathbf{k}+\mathbf{K}_3)\|b)$ $\times[(\mathbf{k}+\mathbf{K}_3)_x$ $\times(\mathbf{k}+\mathbf{K}_3)_y$ $/\|\mathbf{k}+\mathbf{K}_3\|^2]\ F_{-1\text{-}1\text{-}1}$	$B_2 j_2(B_1\|(\mathbf{k}+\mathbf{K}_3)\|b)$ $\times[(\mathbf{k}+\mathbf{K}_3)_y$ $\times(\mathbf{k}+\mathbf{K}_3)_z$ $/\|\mathbf{k}+\mathbf{K}_3\|^2]\ F_{-1\text{-}1\text{-}1}$	$B_2 j_2(B_1\|(\mathbf{k}+\mathbf{K}_3)\|b)$ $\times[(\mathbf{k}+\mathbf{K}_3)_z$ $\times(\mathbf{k}+\mathbf{K}_3)_x$ $/\|\mathbf{k}+\mathbf{K}_3\|^2]\ F_{-1\text{-}1\text{-}1}$	$B_2 j_2(B_1\|(\mathbf{k}+\mathbf{K}_3)\|b)$ $\times[((\mathbf{k}+\mathbf{K}_3)_x^2$ $-(\mathbf{k}+\mathbf{K}_3)_y^2)$ $/(2\|\mathbf{k}+\mathbf{K}_3\|^2)]$ $\times F_{-1\text{-}1\text{-}1}$	$B_2 j_2(B_1\|(\mathbf{k}+\mathbf{K}_3)\|b)$ $\sqrt{3}/6(3(\mathbf{k}+\mathbf{K}_3)_z^2$ $/\|\mathbf{k}+\mathbf{K}_3\|^2 - 1)$ $\times F_{-1\text{-}1\text{-}1}$
$B_2 j_2(B_1\|(\mathbf{k}+\mathbf{K}_4)\|b)$ $\times[(\mathbf{k}+\mathbf{K}_4)_x$ $\times(\mathbf{k}+\mathbf{K}_4)_y$ $/\|\mathbf{k}+\mathbf{K}_4\|^2]\ F_{-1\text{-}11}$	$B_2 j_2(B_1\|(\mathbf{k}+\mathbf{K}_4)\|b)$ $\times[(\mathbf{k}+\mathbf{K}_4)_y$ $\times(\mathbf{k}+\mathbf{K}_4)_z$ $/\|\mathbf{k}+\mathbf{K}_4\|^2]\ F_{-1\text{-}11}$	$B_2 j_2(B_1\|(\mathbf{k}+\mathbf{K}_4)\|b)$ $\times[(\mathbf{k}+\mathbf{K}_4)_z$ $\times(\mathbf{k}+\mathbf{K}_4)_x$ $/\|\mathbf{k}+\mathbf{K}_4\|^2]\ F_{-1\text{-}11}$	$B_2 j_2(B_1\|(\mathbf{k}+\mathbf{K}_4)\|b)$ $\times[((\mathbf{k}+\mathbf{K}_4)_x^2$ $-(\mathbf{k}+\mathbf{K}_4)_y^2)$ $/(2\|\mathbf{k}+\mathbf{K}_4\|^2)]$ $\times F_{-1\text{-}11}$	$B_2 j_2(B_1\|(\mathbf{k}+\mathbf{K}_4)\|b)$ $\sqrt{3}/6(3(\mathbf{k}+\mathbf{K}_4)_z^2$ $/\|\mathbf{k}+\mathbf{K}_4\|^2 - 1)$ $\times F_{-1\text{-}11}$

where B_2 is some hybridization strength, B_1 corresponds to the peak position of the radial function, $b = 8a/(2\pi)$, and $j_2(x)$ denotes the spherical Bessel function for angular momentum $l = 2$:

$$j_2(x) = 3/x^3(\sin x - x\cos x) - \sin x/x.$$

Parameters used in this calculation are given in Table 1 [13]. Thus obtained band structure is shown in Fig. A1, which is consistent with Refs. [13, 20].

Table 1 Parameters for the Ni band structure [13].

β = -8.8 eV	A_1 = 0.25 eV
α = 0.204937 eV	A_2 = 0.106250 eV
V_{111} = 2.036977 eV	A_3 = 0.121385 eV
V_{200} = -0.38744 eV	A_4 = 0.152923 eV
E_0 = -0.95 eV	A_5 = 0.015131 eV
Δ = 0.059360 eV	A_6 = 0.103386 eV
σ_{t2g} = 0.2 eV	B_1 = 0.480651 eV
σ_{eg} = 0.05 eV	B_2 = 12.870937 eV

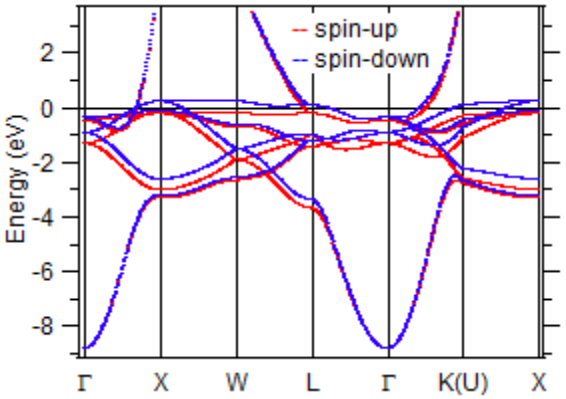

Fig. A1 Semiempirical band structure of Ni along some symmetry lines.

Since the calculation is performed in the 1/48th Brillouin zone, it is convenient to convert the 1/48th BZ to the 1st BZ, in order to show the Fermi surface map, as following the procedures:

(i) The 1/16th zone is obtained from three 1/48th zones:

$$P^{1/48}(x_0, y_0, z_0),\ P^{1'/48} = P^{1/48}(z_0, y_0, x_0),\ \text{and}\ P^{1''/48} = P^{1/48}(z_0, x_0, y_0)$$

$$\text{for } 1 \geq y_0 \geq x_0 \geq z_0 \geq 0.$$

(ii) The 1/8th zone is obtained from two 1/16th zones:

$$P^{1/16}(x_1, y_1, z_1) \text{ and } P^{1'/16} = P^{1'/16}(y_1, x_1, z_1)$$

$$\text{for } 1 \geq y_1 \geq x_1 \geq 0 \text{ and } 1 \geq z_1 \geq 0.$$

(iii) The unit zone is obtained from eight 1/8th zones:

$$P^{1/8}(x_2, y_2, z_2),\ P^{1a/8} = P^{1/8}(-x_2, y_2, z_2),\ P^{1b/8} = P^{1/8}(x_2, -y_2, z_2),$$
$$P^{1c/8} = P^{1/8}(x_2, y_2, -z_2),\ P^{1d/8} = P^{1/8}(-x_2, -y_2, z_2),\ P^{1e/8} = P^{1/8}(x_2, -y_2, -z_2),$$
$$P^{1f/8} = P^{1/8}(-x_2, y_2, -z_2),\ \text{and}\ P^{1g/8} = P^{1/8}(-x_2, -y_2, -z_2)$$

$$\text{for } 1 \geq y_2 \geq 0 \text{ and } 1 \geq x_2 \geq 0 \text{ and } 1 \geq z_2 \geq 0.$$

Thus obtained Fermi surface maps of Ni(111) taken with various photon energies are

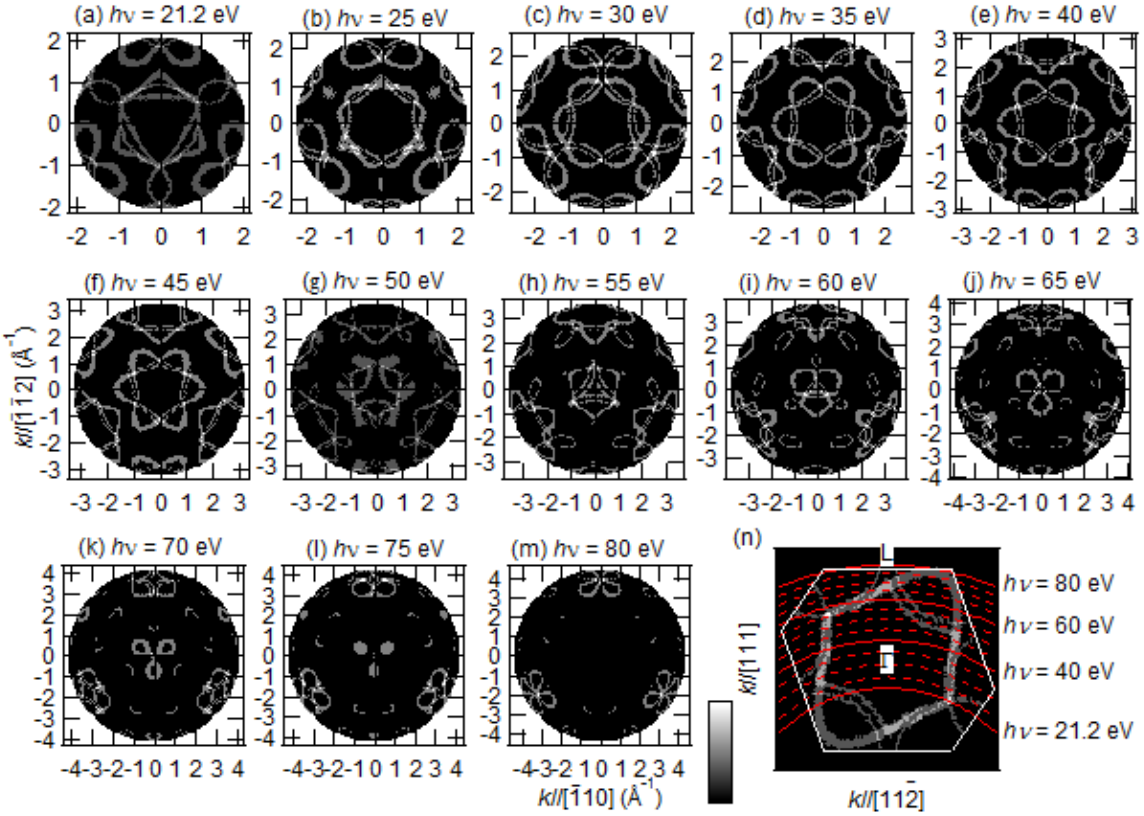

Fig. A2 Photon energy dependent Fermi surfaces of Ni(111). (a) $h\nu$ = 21.2 eV. (b) $h\nu$ = 25 eV. (c) $h\nu$ = 30 eV. (d) $h\nu$ = 35 eV. (e) $h\nu$ = 40 eV. (f) $h\nu$ = 45 eV. (g) $h\nu$ = 50 eV. (h) $h\nu$ = 55 eV. (i) $h\nu$ = 60 eV. (j) $h\nu$ = 65 eV. (k) $h\nu$ = 70 eV. (l) $h\nu$ = 75 eV. (m) $h\nu$ = 80 eV. (n) Traces in k space with the Fermi surface.

shown in Fig. A2. After these procedures, four new *d* orbitals are added to be considered; $|d_{y^2-z^2}>$, $|d_{z^2-x^2}>$, $|d_{3x^2-r^2}>$, and $|d_{3y^2-r^2}>$, which are expressed by the linear combination of the basis set of the five *d* wave functions as follows:

$$|d_{y^2-z^2}> = -1/2\ |d_{x^2-y^2}> - \sqrt{3}/2\ |d_{3z^2-r^2}>,\ |d_{z^2-x^2}> = -1/2\ |d_{x^2-y^2}> + \sqrt{3}/2\ |d_{3z^2-r^2}>,$$

$$|d_{3x^2-r^2}> = \sqrt{3}/2\ |d_{x^2-y^2}> - 1/2\ |d_{3z^2-r^2}>,\ |d_{3y^2-r^2}> = -\sqrt{3}/2\ |d_{x^2-y^2}> - 1/2\ |d_{3z^2-r^2}>.$$

Thus, the contribution from each atomic orbital to the FS can be evaluated (Fig. 7).

References

[1] D. B. Penn, Phys. Rev. Lett. **42**, 921 (1979).

[2] D. E. Eastman, F. J. Himpsel, and J. A. Knapp, Phys. Rev. Lett. **40**, 1514 (1978).

[3] F. J. Himpsel, J. A. Knapp, and D. E. Eastman, Phys. Rev. B **19**, 2919 (1979).

[4] T. J. Kreutz, T. Greber, P. Aebi, J. Osterwalder, Phys. Rev. B **58**, 1300 (1998).

[5] F. J. Himpsel and D. E. Eastman, Phys. Rev. Lett. **41**, 507 (1978).

[6] T. Okuda, J. Lobo-Checa, W. Auwärter, M. Morscher, M. Hoesch, V. N. Petrov, M. Hengsberger, A. Tamai, A. Dolocan, C. Cirelli, M. Corso, M. Muntwiler, M. Klöckner, M. Roos, J. Osterwalder, and T. Greber, Phys. Rev. B **80**, 180404(R) (2009).

[7] H. Namba, K. Yamamoto, T. Ohta, and H. Kuroda, J. Electron Spectrosc. Relat. Phenom. **88-91**, 707 (1998).

[8] Koji Ogawa, Koji Nakanishi, and Hidetoshi Namba, Solid State Commun. **125**, 517 (2003).

[9] F. Matsui, H. Miyata, O. Rader, Y. Hamada, Y. Nakamura, K. Nakanishi, K. Ogawa, H. Namba, and H. Daimon, Phys. Rev. B **72**, 195417 (2005).

[10] Y. Hamada, F. Matsui, Y. Nozawa, K. Nakanishi, M. Nanpei, K. Ogawa, S. Shigenai, N. Takahashi, H. Daimon, and H. Namba, AIP Conf. Proc. **879**, 547 (2007).

[11] H. Daimon, Rev. Sci. Instrum. **59**, 545 (1988).

[12] N. Takahashi, F. Matsui, H. Matsuda, Y. Hamada, K. Nakanishi, H. Namba, and H. Daimon, J. Electron Spectrosc. Relat. Phenom. **163**, 45 (2008).

[13] F. Weling and J. Callaway, Phys. Rev. B **26**, 710 (1982).

[14] H. Daimon, S. Imada, H. Nishimoto, and S. Suga, J. Electron Spectrosc. Relat. Phenom. **76**, 487 (1995).

[15] T. Grandke, L. Ley, and M. Cardona, Phys. Rev. B **18**, 3847 (1978).

[16] S. Goldberg, C. Fadley, and S. Kono, J. Electron Spectrosc. Relat. Phenom. **21**, 285 (1981).

[17] W. Eberhardt and E. W. Plummer, Phys. Rev. B **21**, 3245 (1980).

[18] N. V. Smith and L. F. Mattheiss, Phys. Rev. B **9**, 1341 (1974).

[19] G. C. Fletcher, Proc. Phys. Soc. Lond. A **65**, 192 (1952).

[20] W. Hübner, Phys. Rev. B **42**, 11553 (1990).